Cancer Cell International

RESEARCH

Open Access

Integrated proteomics and metabolomics analyses reveal new insights into the antitumor effects of valproic acid plus simvastatin combination in a prostate cancer xenograft model associated with downmodulation of YAP/TAZ signaling

Federica Iannelli[1†], Rita Lombardi[2†], Susan Costantini[1], Maria Serena Roca[1], Laura Addi[1], Francesca Bruzzese[2], Elena Di Gennaro[1], Alfredo Budillon[3*] and Biagio Pucci[1]

Abstract

Background Despite advancements in therapeutic approaches, including taxane-based chemotherapy and androgen receptor-targeting agents, metastatic castration-resistant prostate cancer (mCRPC) remains an incurable tumor, highlighting the need for novel strategies that can target the complexities of this disease and bypass the development of drug resistance mechanisms. We previously demonstrated the synergistic antitumor interaction of valproic acid (VPA), an antiepileptic agent with histone deacetylase inhibitory activity, with the lipid-lowering drug simvastatin (SIM). This combination sensitizes mCRPC cells to docetaxel treatment both in vitro and in vivo by targeting the cancer stem cell compartment via mevalonate pathway/YAP axis modulation.

Methods Here, using a combined proteomic and metabolomic/lipidomic approach, we characterized tumor samples derived from 22Rv1 mCRPC cell-xenografted mice treated with or without VPA/SIM and performed an in-depth bioinformatics analysis.

Results We confirmed the specific impact of VPA/SIM on the Hippo–YAP signaling pathway, which is functionally related to the modulation of cancer-related extracellular matrix biology and metabolic reprogramming, providing further insights into the molecular mechanism of the antitumor effects of VPA/SIM.

Conclusions In this study, we present an in-depth exploration of the potential to repurpose two generic, safe drugs for mCRPC treatment, valproic acid (VPA) and simvastatin (SIM), which already show antitumor efficacy in combination, primarily affecting the cancer stem cell compartment via MVP/YAP axis modulation. Bioinformatics

[†]Federica Iannelli and Rita Lombardi contributed equally to this work.

*Correspondence:
Alfredo Budillon
a.budillon@istitutotumori.na.it

Full list of author information is available at the end of the article

analysis of the LC–MS/MS and ^{1}H–NMR metabolomics/lipidomics results confirmed the specific impact of VPA/SIM on Hippo–YAP.

Keywords Drug repurposing, Valproic acid, Simvastatin, Proteomics, Metabolomics, Prostate cancer

Background

Prostate cancer (PCa) is the second most common malignancy in men worldwide [1]. Despite the success of androgen deprivation therapy (ADT) in suppressing tumor growth, most patients invariably progress to castration-resistant metastatic prostate cancer (mCRPC) [2]. Although several specific therapeutic options have been developed, mCRPC remains a condition with a poor prognosis and a median survival of approximately two to three years [3]. Major systemic treatment options for mCRPC patients include taxane-based chemotherapy (docetaxel and cabazitaxel) and androgen receptor target agents such as abiraterone or enzalutamide. Although the use of these drugs has improved clinical outcomes, prolonging lifespan, many patients develop resistance [4]. Thus, novel combination treatment strategies are needed to target signaling pathways involved in mCRPC progression and drug resistance. In a recent study, we suggested the potential to repurpose valproic acid (VPA), an antiepileptic agent with histone deacetylase inhibitor (HDACi) activity, and the lipid-lowering drug simvastatin (SIM), which inhibits HMG-CoA reductase (HMGCR), the first step of the mevalonate pathway (MVP), for mCRPC treatment. Notably, MVP is directly involved in steroidogenesis, and several lines of evidence also support a link between the androgen receptor pathway and PCa [5]. Indeed, several epidemiological studies have suggested that statins can reduce the incidence and mortality of PCa, and direct antitumor effects of statins in PCa models have been reported [6, 7]. Conversely, dysregulated HDAC expression has been reported to be associated with poor prognosis in PCa, and the antitumor effects of HDACis, including VPA, have been shown in PCa models [7–9].

In detail, for the first time, we demonstrated the synergistic antitumor interaction between VPA and SIM and the ability of this combination to sensitize mCRPC cells to docetaxel and to revert docetaxel resistance in both in vitro and in vivo models. Interestingly, we observed a reciprocal ability of both VPA and SIM to target histone acetylation and HMGCR expression, strengthening our hypothesis of a synergistic interaction between these drugs [7]. Moreover, we demonstrated the ability of the VPA/SIM combined approach to target cancer stem cell (CSC) compartments through the inhibition of the oncogene Yes-associated protein (YAP), a transcriptional regulator whose hyperactivation is a hallmark of several solid tumors, including PCa, which is essential for cancer initiation/growth and drug resistance [7, 10, 11]. Mechanistically, we demonstrated that the VPA/SIM combination downregulated YAP oncogene expression and activity through the concurrent modulation of MVP and the key cellular metabolic sensor AMP-activated protein kinase (AMPK). In the present study, to further investigate the mechanism of the unique antitumor effect of VPA plus SIM combination, we used liquid chromatography–tandem mass spectrometry (LC–MS/MS) shotgun proteomics to analyze tumor tissues obtained in an in vivo experiment from our study reported above [7]. Specifically, we analyzed tumor tissues from a 22Rv1 PCa cell xenograft model and identified proteins that were differentially expressed between the untreated and VPA/SIM-treated groups. Notably, this approach confirmed the specific impact of VPA/SIM on Hippo–YAP signaling and revealed the ability of this combination treatment to modulate biological processes associated with the extracellular matrix (ECM) and metabolic pathways. Utilizing the same tumor tissue samples, we performed metabolomics and lipidomics analyses using a proton nuclear magnetic resonance (^{1}H-NMR) approach, confirming the metabolic reprogramming induced by VPA/SIM combined treatment (Additional file 1).

Overall, our study provides new insights into the mechanisms underlying the antitumor effects of the VPA/SIM combination, suggesting that this approach can be extended to other cancer models in combination with standard anticancer therapies.

Methods

Shotgun proteomics of tumor samples

Tumor samples were collected from 22Rv1 xenograft tumors. Briefly, five-week-old female NOD/SCID athymic mice (Charles River, Wilmington, MA, USA) were injected subcutaneously with 22Rv1 cells and randomly assigned to receive VPA/SIM in combination (200 mg/kg and 2 mg/kg, respectively, i.p. daily for 2 weeks) or vehicle. This study was performed in compliance with institutional guidelines and regulations (Directive 2010/63/EU; Italian Legislative Decree DLGS 26/2014) and after approval from the appropriate institutional review board (N.865/2015-PR). Untreated xenograft tumors grew rapidly and reached the endpoint size within 3 weeks; at this time, the VPA/SIM combination significantly inhibited tumor growth, and tumors from both groups were collected [7]. For proteomic analysis, tumor samples were lysed with 0.2% RapiGest SF (Waters, MA, USA) in 50 mM ammonium bicarbonate using a Tissue Lyser II system (Qiagen, Hilden, Germany). After the samples

were centrifuged for 30 min at 14,000 rpm at 4 °C, the supernatants were lysed on ice for 2 h, denatured at 80 °C for 15 min and then sonicated. The amount of protein was evaluated by the Bradford assay. A total of 20 µg of total protein was reduced with 10 mM dithiothreitol and then alkylated with 24 mM iodoacetamide at 37 °C for 1 h (Sigma Aldrich, Merck KGaA, Germany). Afterward, protein digestion was performed using trypsin at a 1:50 ratio w/w (Promega Corporation, Madison, WI, USA). The samples were desalted with a C18 resin tip (Millipore, Merck KGaA, Munich, Germany) and dried in a vacuum system. Approximately 5 µg of peptide was resuspended in 0.1% trifluoroacetic acid and injected into a Dionex UltiMate 3000 nanosystem (Thermo Fischer Scientific, CA, USA) coupled with an AmaZon ETD mass spectrometer (Bruker Daltonics, Bremen, Germany). Peptide samples were loaded onto a Pepmap precolumn (2 cm × 100 µm, 5 µm), followed by separation on a 25 cm nanocolumn (0.075 µm, Acclaim PepMap100, C18, Thermo Fischer Scientific, CA, USA) at a flow rate of 300 nL/min. Multistep 360-min gradients of ACN were used. The mass spectrometer equipped with a nanoBooster-CaptiveSpray™ ESI source was operated in data-dependent acquisition mode. For MS generation, enhanced resolution and a trap ICC value of 400,000 were used; for MS/MS acquisition, the ICC target was increased to 1,000,000. CID MS/MS fragmentation was set to the twenty most abundant MS peaks (top 20). The obtained chromatograms were generated using Compass Data Analysis™ v.4.2 (Bruker Daltonics, Bremen, Germany), and the resulting mass lists were processed with the Mascot search engine (v.2.7.0). The database search was restricted to the human SwissProt database. Trypsin as an enzyme, carbamidomethyl (C) as a fixed modification and oxidation (M) as a variable modification were set as the search parameters. The mass tolerances for all identifications were generally fixed at 2 Da for the precursor ions and 0.8 Da for the product ions. Data were filtered using a global FDR < 5%, and only proteins with at least one unique identical peptide sequence (p value < 0.05) were considered identified [12].

Protein quantification analysis

Progenesis QI for Proteomics v. 4.2 (Nonlinear Dynamics, Newcastle, England) was used as a label-free quantification platform. Briefly, the raw data were imported, and the ion intensity maps of all the runs (4 for the CTR group and 3 for the VPA/SIM group) were used for the alignment process. Only alignment scores above 60% were accepted. Peak peaking was performed using the default sensitivity, and a peak width of 0.15 min and charge states of +2, +3 and +4 were used. The survey scan data were used for the quantification of peptide ions without MS/MS data. The data were then normalized to all proteins. Protein identification was achieved using Mascot. Protein abundance was calculated using the sum of all unique peptide normalized ion abundances for that protein in each run [13]. To indicate statistical peptide significance, we considered a fold change greater than 2 if it was associated with a p value ≤ 0.05 (ANOVA), as suggested by Progenesis. In addition, we also considered the false discovery rate (FDR)-adjusted p value, named the q value (≤ 0.01). The technical variability of each peptide/protein was estimated among replicates from the pooled sample by calculating Pearson correlation coefficients (PCCs) using Perseus (v. 1.6.6.0) [14].

Immunoblotting

Protein extraction from xenograft tumor samples is described in Sect. *2.1*. Approximately 50 µg of lysate was resolved by SDS–PAGE as previously described [15]. Western blots were quantified using ImageJ software (Rasband, W.S., U.S., National Institutes of Health, Bethesda, Maryland, USA). The primary antibodies used were as follows: Phospho-LATS1 (Thr1079) (D57D3) rabbit mAb#8654 (Cell Signaling Technology; Leiden, Netherlands). The anti-LATS1 antibody (ab70562) was purchased from Abcam (Cambridge, UK). β-actin C4 (sc-47778) was purchased from Santa Cruz Biotechnology, Inc. (Dallas, TX, USA). The secondary antibodies used were as follows: polyclonal swine anti-rabbit immunoglobulins/horseradish peroxidase (HRP)-linked IgG secondary from Abcam (Cambridge, UK).

Functional annotation analysis

Gene Ontology (GO) enrichment and pathway analyses were performed using the Database for Annotation, Visualization and Integrated Discovery (DAVID) v6.8 (https://david.ncifcrf.gov/) [16]. g: Profiler (version e94_eg41_p11) analyses were performed as follows: GO analyses (GO molecular function (GO: MF), GO cellular component (GO: CC), and GO biological process (GO: BP)) were carried out sequentially. The biological pathways were identified using the WikiPathways (WP) database [17]. The enrichment analysis was performed against Reactome version 66 (https://reactome.org/PathwayBrowser). The networks between MS-identified proteins whose expression levels changed were obtained using Ingenuity Pathway Analysis (IPA) software (GeneGo Inc., St. Joseph, MI, USA), which visualizes proteins as hubs and the relationships between proteins as edges.

Extraction of the polar and lipidic fractions from tumor samples and ^{1}H-NMR metabolomic/lipidic analysis

The tissues (100 mg) from the three untreated and treated groups were subjected to chemical extraction in methanol, chloroform and water to separate the polar and lipidic fractions. The lipidic fractions were dissolved in

700 µL of $CDCl_3$, and the polar fractions were dissolved in 630 µL of PBS-D_2O and 70 µL of 3-(trimethylsilyl)-1-propanesulfonic acid (1% in D_2O) as the internal standard. The ^1H spectra of these polar and lipidic fractions were acquired at 300 K by a 600 MHz Bruker spectrometer equipped with a TCI cryoprobe for 256 and 512 scans, respectively.

Statistical analysis

The statistics of the shotgun proteomics experiment were generated using Progenesis QI for Proteomics v. 4.2 and are reported in each specific section. Representative results from a single western blot analysis experiment are presented; additional experiments yielded similar results.

All the NMR spectral regions were bucketed using the AMIX package (Bruker, Biospin GmbH, Rheinstetten, Germany) and normalized to the total spectrum area with Pareto scaling. Partial least squares-discriminant analysis (PLS-DA) and loading plots generated using the MetaboAnalyst v5.0 tool [18] were performed to compare the spectra obtained from the untreated and treated samples.

Results

Proteomic profiling of prostate xenograft tumor samples

Label-free proteomic analysis was applied to identify and quantify proteins whose abundances significantly differed between untreated- (CTR) and VPA/SIM-treated mouse tumor samples, as described in Fig. 1A. Progenesis software was used to quantify 1030 proteins using the following filters: fold change ≥ 2 and ANOVA test p value ≤ 0.05 (Additional file 2). Among these proteins, 424 were upregulated and 606 were downregulated following VPA/SIM treatment.

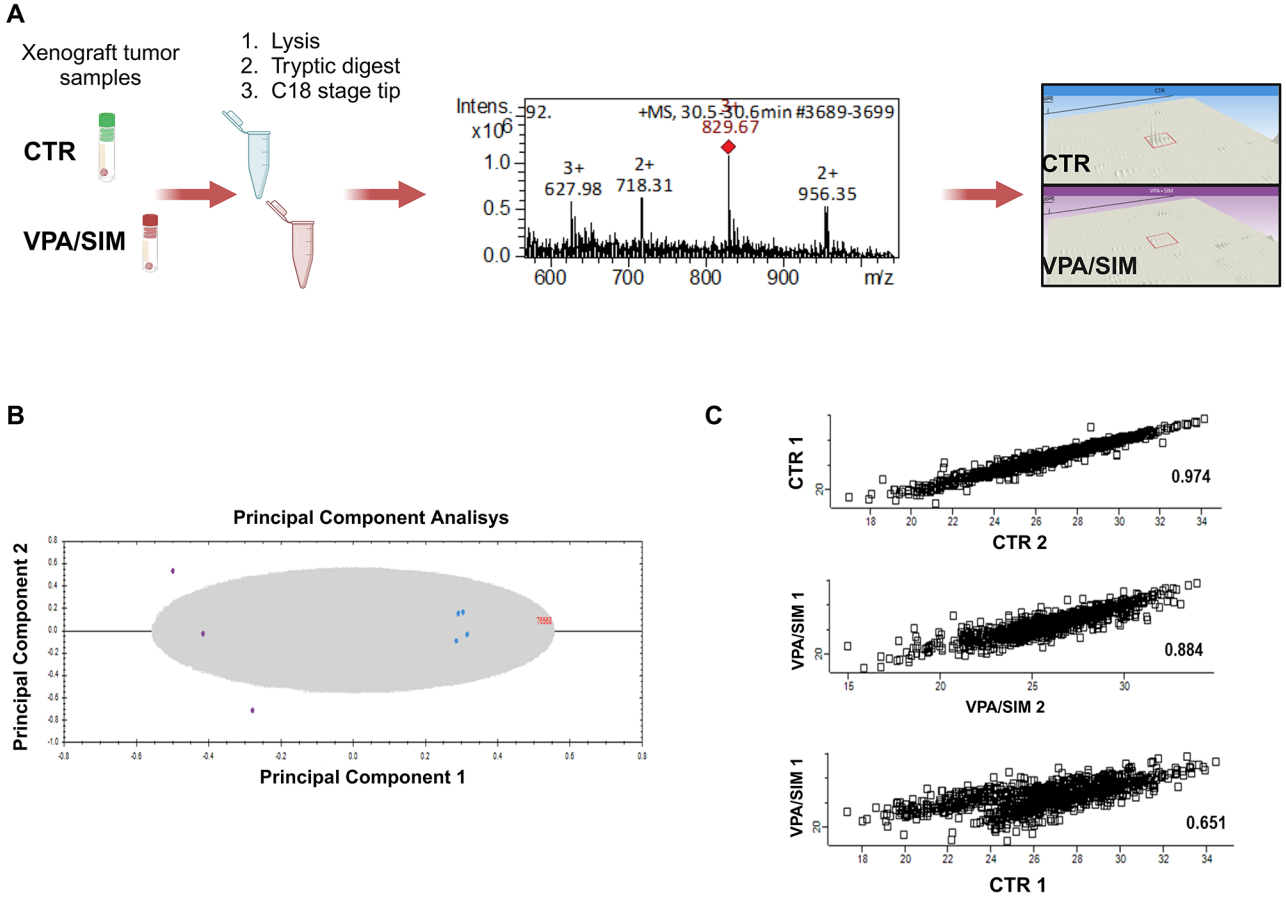

Fig. 1 Schematic representation of the label-free LC–MS/MS-based protein quantification workflow. **(A)** Digested peptides from 22Rv1 xenograft tumor samples treated with VPA/SIM (treated group) or the control (CTR) are depicted. Peptide profiles are aligned, and their intensities are quantified using Progenesis QI for Proteomics software and visualized through 3D ion peak intensity views. The statistical significance of the peptides was determined by ANOVA (p value < 0.05), false discovery rate (FDR)-adjusted q values (q < 0.05), and the criterion of a fold change (FC) ≥ 2. **(B)** Unsupervised multivariate analysis of proteomic data conducted using a principal component analysis (PCA) plot. This analysis visualizes the variation among biological replicates of 22Rv1 CTR (represented by light blue circles) and VPA/SIM-treated 22Rv1 (represented by purple circles), which were generated with Progenesis QI for Proteomics software. **(C)** Biological variability among peptide/protein replicates was assessed by calculating Pearson correlation coefficients using Perseus software (v.1.6.6.0). An absolute value close to 1 indicates a strong linear relationship between replicates. The figure was created using https://www.BioRender.com

A principal component analysis (PCA) plot derived from unsupervised multivariate analysis of differential protein expression profiles demonstrated close correlations between the spot maps of the biological replicates, thus highlighting the experimental reproducibility (Fig. 1B). Furthermore, the Pearson correlation coefficients revealed high reproducibility of peptide/protein levels among control biological replicates (CTR_1 vs CTR_2) and treated biological replicates (VPA/SIM_1 vs VPA/SIM_2). Conversely, CTR_1 vs VPA/SIM_1 analysis revealed a lower correlation coefficient, which was in accordance with the reported differential protein expression between the two groups (Fig. 1C).

Hippo-Yap signaling is one of the main enriched pathways modulated by the VPA/SIM combination

Pathway enrichment analysis of the 1030 differentially expressed proteins was carried out with g: Profiler software, which highlighted, among other factors, epigenetic and histone modifications, thus confirming the effects of VPA activity on tumor cells, as well as AR signaling, extracellular matrix and cytoskeleton targeting, and metabolic pathway engagement (Fig. 2A). Notably, Hippo–YAP signaling emerged as one of the main enriched pathways modulated by VPA/SIM treatment, confirming our previous results [7]. In detail, as reported by the normalized abundance calculated based on peptide ion signal peak intensity, we detected the clear downregulation of YAP and its targets CTGF, CycD1 and ANKH1 in the VPA/SIM vs CTR groups (Fig. 2B). Interestingly, we also observed the downregulation of the TEA domain (TEAD), a transcription factor that directly mediates YAP-induced gene expression, along with the upregulation of 14-3-3, a protein responsible for YAP cytoplasmic retention and degradation following its phosphorylation at Ser127 (Fig. 2B). In the VPA/SIM-treated tumor samples, we also detected the upregulation of YAP upstream negative regulators such as LATS1 and AMPK (Fig. 2C).

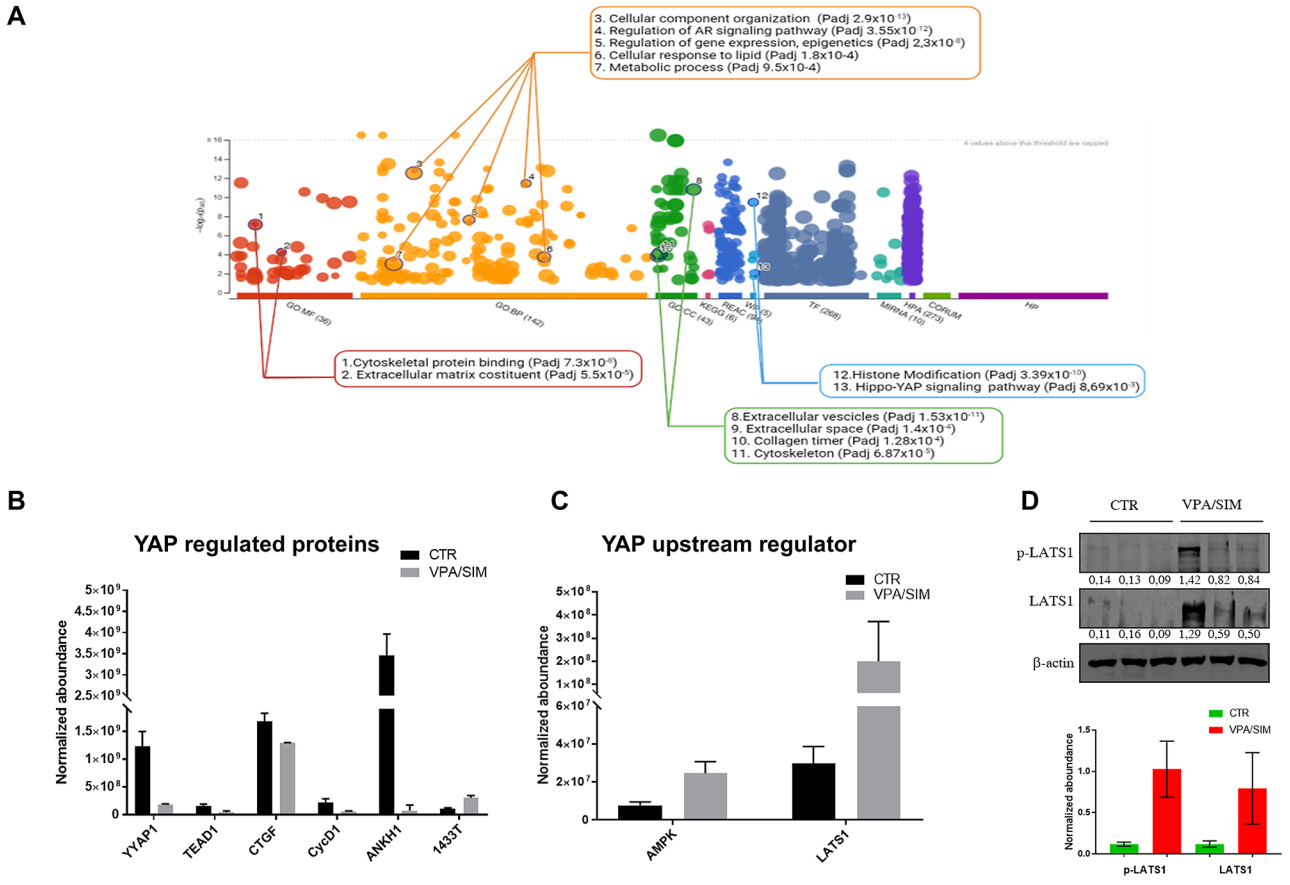

Fig. 2 Functional enrichment analysis using g: Profiler software (version e94_eg41_p11) and western blot analysis. **(A)** The significantly enriched terms according to the GO and WikiPathways (WP) databases. Statistical significance was determined using a threshold of $p < 0.05$. **(B-C)** The normalized abundance values were derived from Progenesis QI for Proteomics software, which quantifies proteins on the basis of peptide ion signal peak intensity. The criteria for significance included a p value < 0.05, a q value < 0.05, and a fold change (FC) ≥ 2. **(D)** Western blot analysis of phospho-LAT1 (pLATS1) and LATS1 in lysates from three representative xenograft tumor samples from treated and control groups. β-actin served as a loading control. Western blot quantifications were performed with ImageJ software. Densitometric analysis values are reported as ratios relative to the corresponding β-actin levels. The graph represents the means +/- SD of the values for pLATS1 and LATS1 in treated and control groups. The figure was created using https://www.BioRender.com

LATS1 represents the last effector of the Hippo–YAP pathway that, upon its phosphorylation at tyrosine 1097, inactivates YAP. Thus, we investigated LATS1 expression and phosphorylation at tyrosine 1097 in tumor lysates from mice treated with the VPA/SIM combination by western blotting and confirmed both increased expression and 1097 phosphorylation (Fig. 2D).

Novel molecular mechanism of the effect of the VPA/SIM combination associated with ECM reorganization

Next, functional annotation analyses were performed to establish the biological processes associated with the 1030 differentially expressed proteins by Gene Ontology (GO) enrichment analysis using DAVID software (Fig. 3). The most relevant enriched GO terms are reported in Fig. 3A. Among the twenty-one GO biological processes selected, eight were associated with cell architecture and cytoskeleton organization, including "regulation of cell junction assembly" and "actin filament reorganization" as the two top processes selected, as well as extracellular matrix (ECM) organization and disassembly, which is consistent with the enriched pathway analysis results reported above. Notably, several proteins associated with these last biological processes, such as calpain-2 catalytic subunit (CAN2), calpain-1 catalytic subunit (CAN1), calpain-1 catalytic subunit (CPNS1), elastin (ELN), matrix metalloproteinase 1 (MMP1), matrix metalloproteinase 10 (MMP10), laminin subunit gamma-1 (LAMC1),

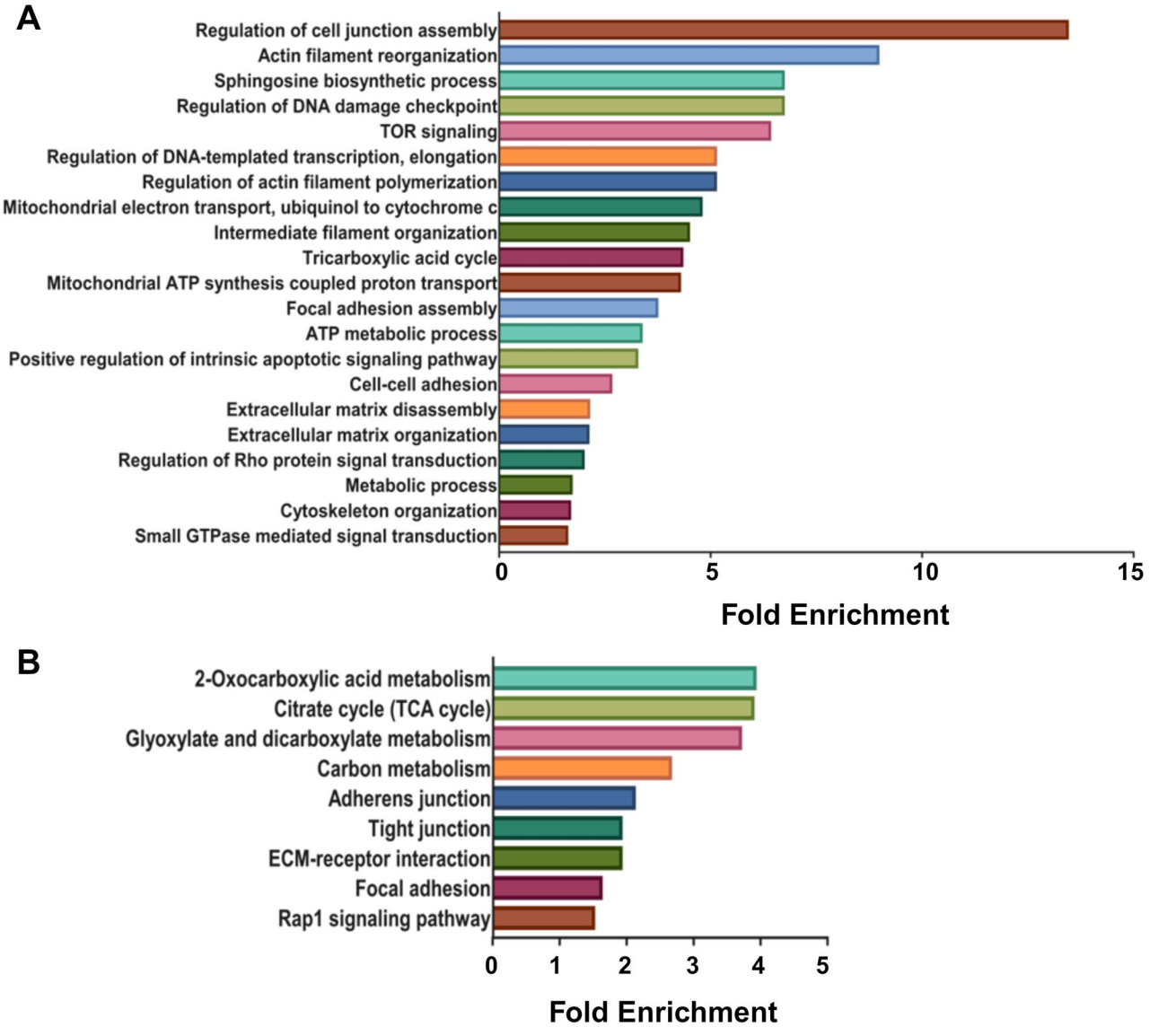

Fig. 3 Gene Ontology (GO) enrichment and pathway analyses were performed using the Database for Annotation Visualization and Integrated Discovery (DAVID) v6.8 (https://david.ncifcrf.gov/). **(A)** Gene Ontology (GO) biological process and **(B)** Kyoto Encyclopedia of Genes and Genomes (KEGG) pathway analyses. Statistical significance was determined using a threshold of $p < 0.05$. The figure was created using https://www.BioRender.com

periostin (POSTN), Ras-related protein Rab-11 A (RB11A), microtubule-associated protein 2 (MTAP2), protein-tyrosine phosphatase mu (PTPRM) and serine/threonine-protein kinase Unc-51-like kinase 1 (ULK1), were reduced in VPA/SIM-treated tumor samples (Table 1). Notably, these proteins, in addition to their structural roles, are involved in several pathways influencing tumor growth and progression [19–27].

For each protein, we reported the gene and protein names, accession numbers from the UniProt database and fold changes obtained by comparing the mean normalized peptide ion signal peak intensities in the 22Rv1 VPA/SIM-treated and CTR groups (Table 1).

ECM-related proteins are directly associated with YAP in one main network

Interestingly, increased ECM stiffness promotes cell spreading, the nuclear localization of YAP and the upregulation of its target genes [28]. Thus, we hypothesized that the ECM remodeling and YAP modulation induced by the VPA/SIM combination could be functionally related. To address this hypothesis, we interrogated the Ingenuity Pathway Analysis (IPA) results, looking for direct interactions, and found that 11 out of the 12 identified proteins closely clustered together and with YAP. Specifically, "Metastasis of cells", "Morphology of malignant tumor", "Proliferation of stem cells, mesenchymal stem cells and connective tissue cells", "Differentiation of tumor cells", "Angiogenesis", "Migration of tumor cell lines, prostate cancer cell lines and carcinoma cell lines" and "Invasion of tumor cell lines" were the IPA-predicted top molecular and cellular functions (Fig. 4).

VPA/SIM combination-induced dysregulation of metabolic processes

After the cell architecture/cytoskeleton and ECM organization processes, the most represented biological processes highlighted by both functional and GO enrichment analyses were related to metabolic pathways (Figs. 2A and 3A).

An additional in-depth analysis investigating Kyoto Encyclopedia of Genes and Genomes (KEGG) pathways also confirmed a number of metabolism associated pathways involved in the differential protein expression profiles between untreated and VPA/SIM-treated tumor tissue samples (Fig. 3B).

Among the proteins involved in metabolic processes, enoyl-CoA hydratase (ECHD2) and 3-hydroxyacyl-CoA dehydrogenase type-2 (HCD2), which are involved in the second and third steps of the beta-oxidation pathway of fatty acid metabolism, were downregulated and upregulated in the VPA/SIM-treated group, respectively (Table 1).

Table 1 Top Biological Processes and associated proteins modulated in VPA/SIM-treated tumor samples

Biological Process	Gene names	Protein names	UniProt Accession numbers	Fold- change VPA + SIM/ CTR
Cell architecture and cytoskeleton organization	CAN2	Calpain-2 catalytic subunit	P17655	-3.58
	CAN1	Calpain-1 catalytic subunit	P07384	-7.74
	CPNS1	Calpain small subunit	P04632	-2.40
	ELN	Elastin	P15502	-3.90
	MMP1	Matrix metalloproteinase 1	P03956	-5.06
	MMP10	Matrix metalloproteinase 10	P09238	-2.12
	LAMC1	Laminin subunit gamma-1	P11047	-4.75
	POSTN	Periostin	Q15063	-2.73
	RB11A	Ras-related protein Rab-11 A	P62491	-4.16
	MTAP2	Microtubule-associated protein 2	P11137	-4.14
	PTPRM	Protein-tyrosine phosphatase mu	P28827	-8.60
	ULK1	Serine/threonine-protein kinase ULK1	O75385	-42.92
Biological Metabolic Process	HCD2	3-hydroxyacyl-CoA dehydrogenase type-2	Q99714	+2.01
	ECHD2	Enoyl-CoA hydratase	Q86YB7	-2.92
	MDH1	Malate dehydrogenase, cytoplasmic	P40925	+2.33
	MDH2	Malate dehydrogenase, mitochondrial	P40926	+7.03
	SDHA	Succinate dehydrogenase, mitochondrial	P31040	+6.93
	ACON	Aconitate hydratase, mitochondrial	Q99798	+3.32
	CISY	Citrate synthase, mitochondrial	O75390	-2.84
	ENOA	Alpha-enolase	P06733	+2.88
	ALDOA	Fructose-bisphosphate aldolase A	P04075	+2.89
	ASGL1	Isoaspartyl peptidase/L-asparaginase	Q7L266	-2.67
	G6PI	Glucose-6-phosphate isomerase	P06744	+3.44

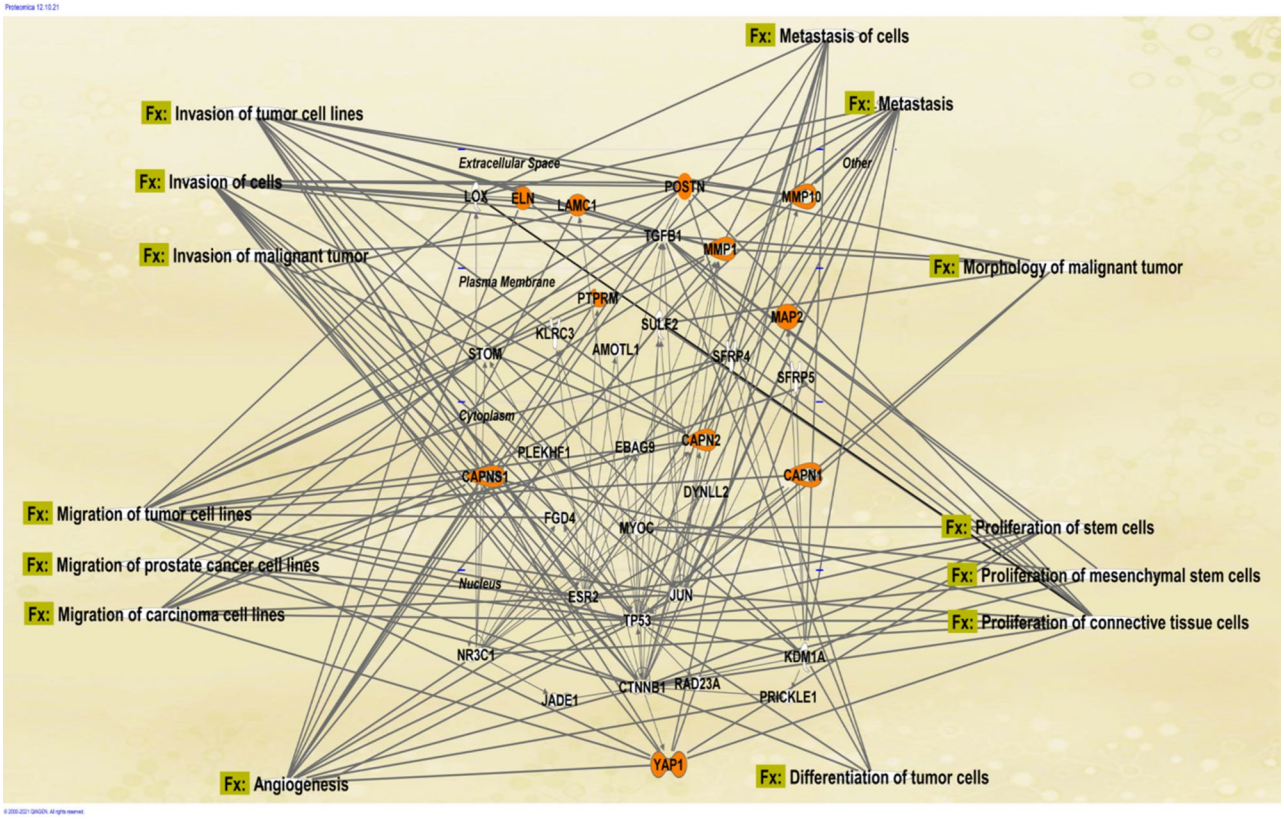

Fig. 4 Interactomic analysis using Ingenuity Pathway Analysis (IPA) software. Interactomic analysis was performed using Ingenuity Pathway Analysis (IPA) software to visualize protein networks, where proteins are depicted as hubs and their relationships as edges. This figure illustrates a network identified by IPA, highlighting direct interactions involving 11 out of 12 identified proteins (shown in orange). The molecular functions (Fx) associated with the proteins within the network are reported. The figure was created using https://www.BioRender.com

Moreover, among the most representative biological metabolic processes modulated by VPA/SIM is the tricarboxyloic acid cycle (TCA). Specifically, in VPA/SIM-treated tumors, we observed increased expression of mitochondrial aconitase (ACON) (Table 1), which catalyzes the interconversion of citrate to isocitrate in the second step of the TCA cycle [29] (Fig. 6). Conversely, we detected lower expression of citrate synthase (CISY), a rate-limiting enzyme in the citrate cycle that is capable of catalyzing the conversion of oxaloacetate and acetyl-CoA to citrate. Furthermore, we found that both cytosolic and mitochondrial malate dehydrogenases (MDH1 and MDH2, respectively) were upregulated in the VPA/SIM-treated group. Finally, mitochondrial succinate dehydrogenase (SDHA), which has the unique ability to participate in both the citric acid cycle and the electron transport chain, was also upregulated by the treatment. This enzyme, which is embedded in the inner mitochondrial membrane, performs the chemical reaction that produces fumarate from succinate.

Voronoi diagram visualization by Reactome analysis confirmed that several pathways were grouped according to the relationships in "metabolism pathway", including "metabolism of lipid pathway" as a contiguous region (Additional file 3) [30].

Treatment with the VPA/SIM combination influenced the metabolomics and lipidomics profiling

To confirm the impact of the modulated enzymes indicated above, we performed ^{1}H-NMR spectroscopy to evaluate the metabolomics/lipidomics profiles of the same tissue samples from untreated and VPA/SIM-treated tumors. As reported in Fig. 5A, multivariate statistical analysis revealed a marked difference between the treated and control samples, with a total variance equal to 59.2%. The loading plot illustrated in Fig. 5B shows the significant modulation of several metabolites, such as amino acids, intermediates of the TCA cycle, the urea cycle and glycolysis. Specifically, the levels of citrate, sarcosine, ATP, malate, glucose, aspartate, and citrulline decreased, whereas only the ornithine level increased after VPA/SIM treatment (Fig. 5B).

Interestingly, the lower levels of citrate correlated with the lower levels of CISY and the higher levels of ACON reported above, as also suggested elsewhere [31]. Moreover, the lower levels of malate correlated with

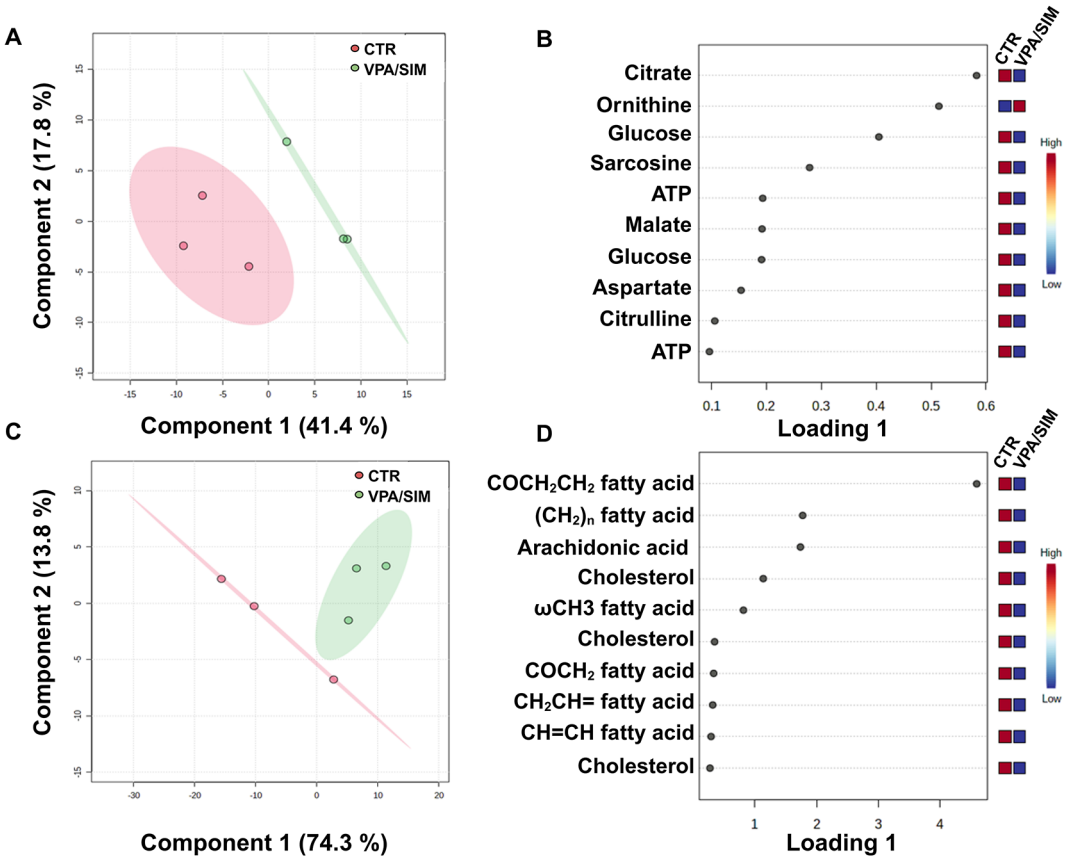

Fig. 5 Score and loading plots related to 1 H-NMR analysis. Polar **(A-B)** and lipidic **(C-D)** fractions obtained by the partial least squares-discriminant analysis (PLS-DA) algorithm were used to compare the spectra obtained for the 22Rv1 VPA/SIM-treated and CTR groups to explain the maximum separation between the defined class samples in the data. The loading plot is obtained by setting H = K − 1, where H is the number of dimensions and k is the number of variables to select on each dimension. In the loading plots, we highlighted the top ten proton signals of metabolites/lipids that were significantly different between the two analyzed groups. The colored boxes on the right indicate the relative proton signal intensity of the identified metabolites in each group under study. The gradient color scheme ranges from blue color for lower abundance to red color for high abundance. The figure was created using https://www.BioRender.com

the higher levels of malate dehydrogenases (MDHs) we detected in the VPA/SIM-treated group (Table 1). The decrease in glucose levels could be related to the VPA/SIM-induced increases in the expression levels of three enzymes (ALDOA, ENOA and G6PI) involved in glycolysis (Table 1). The parallel clear reduction in ATP also indicated alterations in energy-related pathways. The lower levels of aspartate and the parallel reduction of asparaginase (ASGL1) induced by VPA/SIM might also contribute to the alteration of the TCA cycle. Aspartate also contributes to the urea cycle, where both ornithine and citrulline are involved. In particular, ornithine is a precursor of citrulline that is involved in the production of urea from ammonia (i.e., the urea cycle) and is synthesized itself in the last step of this cycle; this process is catalyzed by arginase, which cleaves arginine to produce urea and ornithine.

Overall, the data from both metabolomics and proteomics analyses confirmed that VPA/SIM treatment may induce metabolic reprogramming and alterations, as illustrated schematically in Fig. 6.

Multivariate statistical analysis of the NMR spectra obtained from the lipid fractions also revealed a marked difference between the treated and control samples, with a total variance equal to 88.1% (Fig. 5C). The loading plot revealed that several proton signals of cholesterol and fatty acids decreased after treatment (Fig. 5D). These results are in agreement with the reduction in cholesterol levels we observed in PCa xenograft tumor samples upon VPA/SIM combination treatment [7] and also correlated with the data reported above. Indeed, both ACON modulation and citrated reduction affect both cholesterol and fatty acid synthesis [32, 33]. Moreover, the decreased levels of fatty acids observed in the VPA/SIM–treated samples can be explained by increased degradation via beta-oxidation, as previously reported to be induced by VPA [34]. Notably, a critical enzyme involved in fatty acid beta-oxidation is HCD2, an enzyme reported by

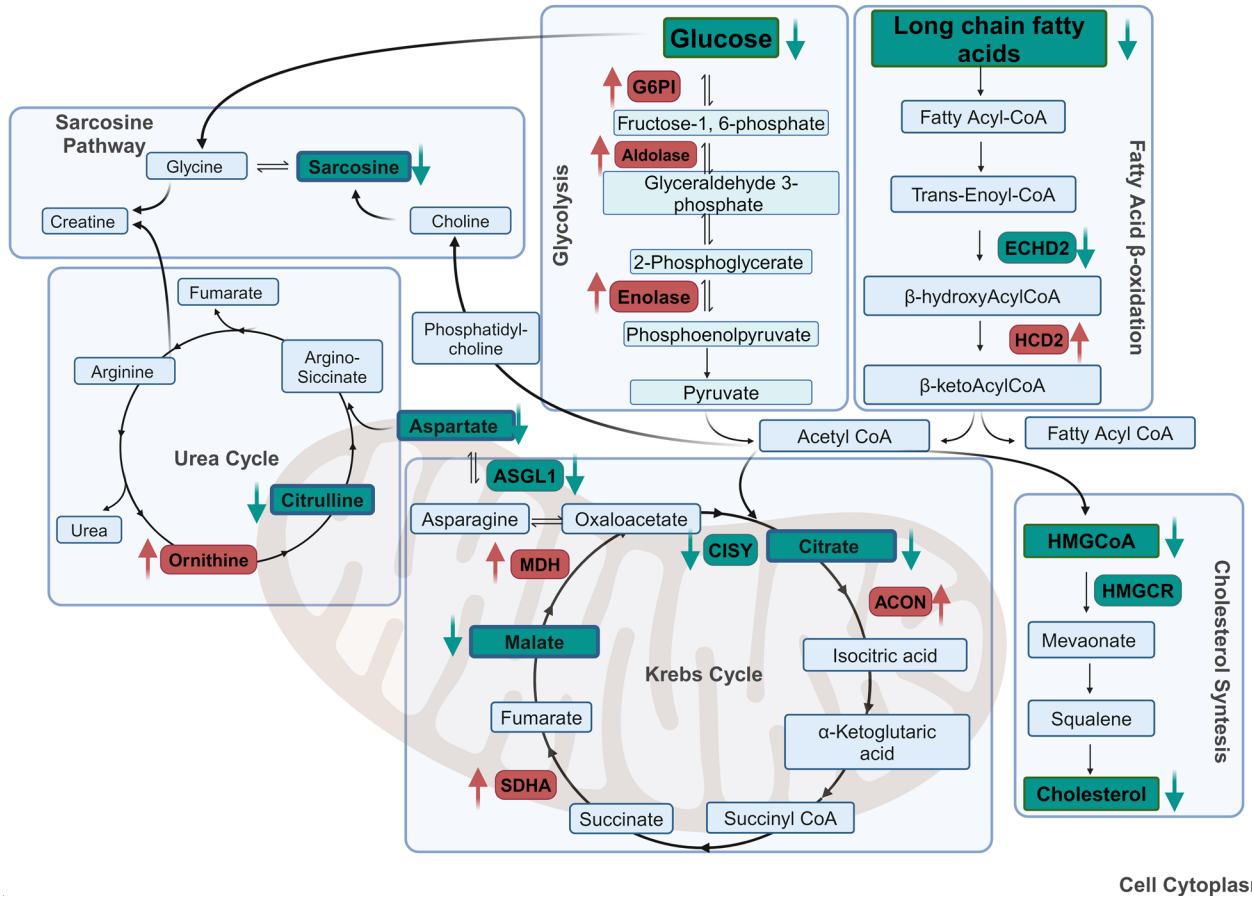

Fig. 6 Schematic representation of the metabolic mechanisms modulated in the 22Rv1 VPA/SIM-treated and CTR groups. Metabolic mechanisms altered in the 22Rv1 xenograft tumor samples treated with VPA/SIM compared with those in the control (CTR) group. The enzymes and metabolites highlighted in red are those whose levels increased, whereas the enzymes highlighted in green are those whose levels decreased in the 22Rv1 VPA/SIM-treated group. The figure was created using https://www.BioRender.com

proteomics analysis to be upregulated by VPA/SIM treatment [34].

Discussion

The integration of multiomics data plays pivotal roles in elucidating the molecular mechanism of tumorigenesis, discovering new biomarkers and identifying drug targets [35]. In the present study, we utilized proteomics and metabolomics approaches to further investigate the mechanism of the antitumor combined effect of two well-known generic drugs, VPA and SIM, along with their ability to potentiate chemotherapy and reverse chemoresistance in prostate tumor models [7]. We analyzed tumor tissues from treated and untreated xenograft mouse models to highlight important physiological processes that are normally lacking in in vitro models, such as angiogenesis or stromal interactions, both of which influence tumor growth and metastasis.

One of the most interesting findings of the present study is the confirmation that the antitumor effects of VPA plus SIM combination involve the modulation of the Hippo signaling pathway, a major player in regulating stem cell and cancer biology through its effectors: YAP and the related other transcriptional regulator, TAZ (transcriptional coactivator with PDZ-binding motif) [36].

Interestingly, YAP, which we confirmed to be downregulated at the protein level by VPA/SIM treatment, as previously described [7], is recognized as a clinical marker for PCa progression and a regulator of mCRPC, correlating with patients' Gleason scores, prostate-specific antigen (PSA) levels and extraprostatic extensions and thus is associated with poor prognosis [11]. When the Hippo pathway is activated, mammalian MST1/2 phosphorylates and activates LATS1/2, which in turn phosphorylates YAP/TAZ at tyrosine or serine residues, inducing YAP/TAZ cytoplasmic retention and inactivation.

Notably, we provided additional insights into the mechanism studied in the previous work, demonstrating the VPA/SIM-induced upregulation of both the protein expression and activity of LATS1 in tumor tissue samples. The oncogenic role of YAP/TAZ mainly

depends on their nuclear localization, where YAP/TAZ interact with TEAD, which we found to be downregulated upon treatment, to form a complex that promotes the expression and activation of downstream target genes [11]. Moreover, the protein 14-3-3, which we found to be upregulated upon treatment, inactivates the proliferative function of phospho-YAP/TAZ by binding and sequestering the protein complex in the cytosol, thus preventing their interaction with TEAD transcription factors [37]. Furthermore, the Ras-related protein Rab11A, which is downregulated by VPA/SIM, has been reported to induce YAP protein expression and inhibit Hippo signaling, thus influencing cell cycle protein expression and cell proliferation [27].

In our previous study, we focused on the critical relationship between YAP and MVP, which relies mainly on CSC behavior and generation in PCa models, and revealed that the VPA/SIM combination was able to downregulate all the principal YAP transcriptional targets, such as CTGF, CYR61, BIRC5 and ANKH1, which are highly enriched in patients with PCa tumors [7]. Interestingly, in our proteomics study, in addition to YAP and TEAD1, YAP targets such as CTGF, CycD1 and ANKH1 were determined to be downregulated in the VPA/SIM tumor xenograft samples compared with the untreated samples.

In line with our results, several studies have suggested that statins modulate YAP phosphorylation, localization and activity. However, some studies have suggested that the effect of statins is independent of MST1/2 and LATS1/2 activity [38, 39], whereas others have described a significant induction of LATS1 expression upon statin treatment [40, 41].

Gene Ontology analysis related to biological processes also identified a substantial group of proteins related to the ECM organization modulated by VPA/SIM compared with that in untreated tumors. The ECM represents a critical part of the tumor microenvironment and it is also essential for the construction of the metastatic niche [42]. Interestingly, we observed VPA/SIM-mediated downregulation of calpains (CAN1, CAN2 and CPNS1), whose expression levels are usually increased in cancer cells, where they can regulate the activation of MMPs for ECM remodeling, angiogenesis, cancer invasion and metastasis [19, 43].

For example, CAN2 can cleave and remove the ligand-binding domain (LBD) from AR, producing a constitutively active form of AR, which contributes to PCa cell aggressiveness [19]. Similarly, overexpression of MMP-1, which we reported to be downregulated by VPA/SIM, has been described in PCa compared with benign prostatic hypertrophy [21]. Moreover, overexpression of POSTN, which is also decreased by VPA/SIM, has been associated with worse baseline clinical features, shorter disease-free survival (DFS), and reduced overall survival (OS) in patients with PCa [25]. Among those differentially expressed proteins downregulated by VPA/SIM cotreatment, MTAP2, another protein of interest in PCa, was identified as a prognostic marker in several cancers and was linked to taxane-based therapy resistance [44]. Finally, the serine/threonine-protein kinase ULK1, which is also downregulated by VPA/SIM, is involved in the AR-regulated signaling cascade that promotes autophagic flux during PCa cell proliferation and survival [45].

Alterations in the mechanical properties of the ECM, represented mainly by stiffness and elasticity, can be induced by cancer cells themselves or by stromal cells and represent mechanical inputs that profoundly affect crucial biological aspects of tumor development, such as cell proliferation, differentiation and apoptosis [46]. Similarly, within cancer cells, the cytoskeleton needs to be continually reorganized to regulate cell shape and movement so that the cells can invade the surrounding tissue, extravasate and reach metastatic sites. Accumulating evidences have demonstrated that YAP/TAZ are primary sensors of the physical nature of a cell, as defined by its structure, shape and polarity [47]. YAP and TAZ also maintain plasticity in cell–ECM adhesion by limiting the maturation of focal adhesions, enabling cell migration [48]. In line with the above observations, we found that the identified ECM proteins were associated with one main IPA network and that all were related to YAP. These results suggested that the VPA/SIM combination influenced ECM reorganization through YAP in our PCa xenograft tumor samples, promoting an unfavorable environment for PCa progression. IPA analysis also revealed that transforming growth factor-beta (TGF-β) was the main hub in the network. Interestingly, in cooperation with YAP/TAZ, TGF-β plays pivotal roles in the production of fibrogenic factors and ECM proteins, which are likely to contribute to cancer progression [49–51]. Moreover, POSTN, a VPA/SIM downregulated protein, is an important mediator of TGF-β-induced EMT and metastatic progression in PCa [52].

In this context, previous studies have reported that statins may impair the tumor metastatic process by inhibiting normal actin polymerization and relative invadopodia formation and attachment to and spread in the ECM, contributing to a reduction in metastatic spread [53–55].

Finally, we demonstrated the impact of VPA/SIM cotreatment on PCa xenograft tumor metabolism by identifying several modulated proteins related to metabolic pathways as well as the modulation of several coordinated metabolites. Interestingly, dysregulation of metabolism has been linked with carcinogenesis and PCa progression [56]. Specific metabolites/enzymes modulated by VPA/SIM treatment are directly associated with PCa

progression and growth. For example, PCa is associated with fatty acid oxidation abnormalities [57], and VPA/SIM downregulates the fatty acid beta-oxidation enzyme ECHD2, the expression of which is correlated with the progression, metastasis and drug resistance of PCa and is considered a potential biomarker for PCa diagnosis [58]. We also demonstrated the impact of VPA/SIM treatment on the TCA cycle, whose dysregulation has also been reported in PCa. For example, decreased expression of CISY, which is downregulated by VPA/SIM, affects PCa cell proliferation, colony formation, migration, invasion and the cell cycle in vitro and inhibits tumor growth in vivo [56]. In addition, CISY downregulation potentially inhibits lipid metabolism and mitochondrial function in PCa cells [56]. Interestingly, decreased CISY activity was observed in patients during simvastatin treatment [59]. Similar results were obtained in rats, in which VPA was able to decrease CISY [60]. Furthermore, germline mutations of the SDH gene, whose protein is upregulated by VPA/SIM, has been identified in several types of cancer and has been shown to contribute to the abnormal accumulation of succinate in the cytosol of tumor cells and in the extracellular fluids of patients. These observations suggest that SDHA can be defined as a tumor suppressor and that succinate is an oncometabolite capable of promoting epithelial-to-mesenchymal transition, angiogenesis stimulation, migration and invasion and amplifying oncogenic cascades [61, 62]. We also demonstrated the VPA/SIM-mediated downmodulation of asparaginase, an enzyme that is overexpressed in CRPC [63].

Similarly, metabolomics and lipidomic analyses demonstrated the significant impact of VPA/SIM treatment on metabolites that were functionally correlated with the modulated pathways reported above. For example, clear decreases in fatty acid and cholesterol levels were reported in PCa xenograft tumor tissues from VPA/SIM-treated mice. In line with our data, Zhang et al. reported that, compared with control rats, rats orally treated with VPA presented decreased levels of free fatty acids and intermediate products of the Krebs cycle, such as arachidonic acid and citrate [64].

Moreover, our analysis revealed lower levels of glucose in the VPA/SIM combination group than in the control group, but this effect was complemented by higher levels of enzymes involved in glycolysis and lower levels of ATP, the final product of glycolysis cues.

In accordance with our data, significant time- and concentration-dependent decreases in glucose levels in lymphoma and colon adenocarcinoma cell lines treated with statins were previously reported [65]. Similarly, VPA treatment significantly decreased plasma glucose in in vivo models [66]. Additionally, several clinical studies reported lower blood glucose levels in VPA-treated patients than in controls [67]. Finally, high levels of sarcosine, which were downregulated by VPA/SIM, were present in the sera of high-grade PCa patients but not in those of low-grade PCa patients [68], as well as in the urine samples of PCa patients during progression [69], and are considered a marker of PCa aggressiveness [70].

Notably, recent findings have implicated YAP in the context of cell metabolism, establishing that YAP/TAZ activity is affected by various metabolic cues, such as glucose, lipids, and metabolites, suggesting that an emerging node coordinates nutrient availability with cell growth and tissue homeostasis [71]. For example, changes in nutrients and oxygen during metastasis may change YAP/TAZ binding partners and coordinate cancer progression and metastasis [72]. Here, we also demonstrated the VPA/SIM-induced upregulation of the expression of AMPK, a key energy sensor and master regulator of cellular metabolism, which directly phosphorylates YAP at multiple sites to impair its activity, as previously demonstrated by our group [7].

Conclusions

Taken together, our findings suggest that VPA and SIM co-treatment inhibits tumor growth and progression, negatively influencing cancer cell cytoskeleton reorganization and the ECM in a complex mechanism involving the regulation of multiple proteins through the inhibition of YAP/TAZ function. We also showed that the VPA/SIM combination was able to target metabolic reprogramming in tumor cells in a mechanism involving the modulation of specific enzyme expression, an effect potentially linked to YAP signaling, confirming its central role in PCa tumorigenesis and as the main target of VPA/SIM. This study significantly expands our understanding of the molecular mechanisms of the combination of these two safe and generic drugs, contributing to the identification of potential biomarkers for patient selection that can benefit from this treatment schedule. Indeed, these findings corroborate the results obtained previously by our group on the repurposing of VPA and SIM association for cancer treatment, an approach that, beyond PCa, could be extended to different cancer types in combination with other anticancer drugs and that merits clinical evaluation.

Abbreviations

^{1}H-NMR	Proton Nuclear Magnetic Resonance
ACON	Aconitase
ADT	Androgen deprivation therapy
ALDOA	Fructose-bisphosphate aldolase A
AMPK	AMP-activated protein kinase
ANKH1	Ankyrin repeat and KH domain-containing protein 1
AR	Androgen Receptor
ASGL1	Asparaginase
ATP	Adenosine triphosphate
CAN1	Calpain-1 catalytic subunit
CAN2	Calpain-2 catalytic subunit
CISY	Citrate synthase

CPNS1	Calpain small subunit
CSCs	Cancer stem cells
CTGF	Connective tissue growth factor
CycD1	Cyclin D1
DFS	Disease-free survival
ECHD2	Enoyl-CoA hydratase
ECM	Extracellular matrix
ELN	Elastin
ENOA	Alpha-enolase
FDR	False discovery rate
G6PI	Glucose-6-phosphate isomerase
GO	Gene Ontology
GO:BP	GO biological process
GO:CC	GO cellular component
GO:MF	GO molecular function
HCD2	3-hydroxyacyl-CoA dehydrogenase type-2
HDACi	Histone deacetylases inhibitors
HMGCR	HMG-CoA reductase
IPA	Ingenuity Pathway Analysis
KEGG	Kyoto Encyclopedia of Genes and Genomes
LAMC1	Laminin subunit gamma-1
LATS1	Large Tumor Suppressor Kinase 1
LBD	Ligand-binding domain
LC-MS/MS	Liquid chromatography-tandem mass spectrometry
mCRPC	Castration-resistant metastatic prostate cancer
MDH1	Cytosolic mitochondrial malate dehydrogenases
MDH2	Mitochondrial malate dehydrogenases
MMP1	Matrix metalloproteinase 1
MMP10	Matrix metalloproteinase 10
MST1/2	Mammalian Ste20-like kinases 1/2
MTAP2	Microtubule-associated protein 2
MVP	Mevalonate pathway; OS: Overall survival
PCA	Principal component plot
PCa	Prostate cancer
PCC	Pearson correlation coefficients
PLS-DA	Partial least squares-discriminant analysis
POSTN	Periostin
PSA	prostate-specific antigen
PTPRM	Protein-tyrosine phosphatase mu
RB11A	Ras-related protein Rab-11 A
SDHA	Mitochondrial succinate dehydrogenase
SIM	Simvastatin
TAZ	Transcriptional coactivator with PDZ-binding motif
TCA	Tricarboxyloic acid cycle
TEAD	TEA domain
TGF-β	Transforming growth factor-beta
ULK1	Unc-51-like kinase 1
VPA	Valproic Acid
WP	WikiPathways
YAP	Yes-associated protein

Supplementary Information

The online version contains supplementary material available at https://doi.org/10.1186/s12935-024-03573-1.

Supplementary Material 1

Supplementary Material 2

Supplementary Material 3: Voronoi diagram representation. Hierarchical pathway overrepresentation analysis of the protein elements identified in the proteomic study using Reactome (https://reactome.org/PathwayBrowser, ver. 66). Statistical significance was determined using a threshold of $p < 0.05$. The figure was created using https://www.BioRender.com

Author contributions

FI, RL, BP, FB, AB were involved in conceptualization; AB was responsible for project funding.FI, RL and MSR were involved in in vivo models, collected and processed tumor samples.FI and LA performed the data validation experiments.RL, BP performed the proteomic experiments and initial data processing. RL, FI, BP performed analysis of the proteomics data. SC performed Metabolomics and Lipidomics experiments and analysis.FI, RL, BP, EDG and AB wrote the manuscript with input from all co-authors.

Funding

This work was supported by Italian Ministry of Health, Ricerca Corrente Funds to Istituto Nazionale Tumori G. Pascale project: Linea 2/2 to AB; and by Regione Campania grants: POR FESR 2014/2020 Progetto Campania Onco-Terapie/CUP: B61G18000470007; POR FESR 2014/2020 del progetto "PREMIO-Infrastruttura Per La Medicina Di Precisione In Oncologia"/CUP: B61C17000080007; POR FESR 2014–2020, del progetto "CIRO-Campania Imaging Infrastructure for Research in Oncology"/CUP: B61G17000190007.

Data availability

Proteomics and metabolomics raw data are available at https://zenodo.org/records/10118913.

Declarations

Ethical approval

Not applicable.

Competing interests

The authors declare no competing interests.

Author details

[1]Experimental Pharmacology Unit, Istituto Nazionale Tumori—IRCCS—Fondazione G. Pascale, Naples 80131, Italy
[2]Experimental Animal Unit, Istituto Nazionale Tumori—IRCCS—Fondazione G. Pascale, Naples 80131, Italy
[3]Scientific Directorate, Istituto Nazionale Tumori—IRCCS—Fondazione G. Pascale, Via M. Semmola, Napoli 80131, Italy

Received: 12 March 2024 / Accepted: 11 November 2024
Published online: 16 November 2024

References

1. Rawla P. Epidemiology of prostate Cancer. World J Oncol. 2019;10(2):63–89.
2. Jang A, Sartor O, Barata PC, Paller CJ. Therapeutic potential of PARP inhibitors in the treatment of metastatic castration-resistant prostate Cancer. Cancers (Basel). 2020;12(11).
3. Mehtala J, Zong J, Vassilev Z, Brobert G, Gabarro MS, Stattin P, et al. Overall survival and second primary malignancies in men with metastatic prostate cancer. PLoS ONE. 2020;15(2):e0227552.
4. Rizzo M. Mechanisms of docetaxel resistance in prostate cancer: the key role played by miRNAs. Biochim Biophys Acta Rev Cancer. 2021;1875(1):188481.
5. Guerrero-Ochoa P, Rodriguez-Zapater S, Anel A, Esteban LM, Camon-Fernandez A, Espilez-Ortiz R et al. Prostate Cancer and the Mevalonate Pathway. Int J Mol Sci. 2024;25(4).
6. Allott EH, Farnan L, Steck SE, Arab L, Su LJ, Mishel M, et al. Statin use and prostate Cancer aggressiveness: results from the Population-based North Carolina-Louisiana prostate Cancer Project. Cancer Epidemiol Biomarkers Prev. 2016;25(4):670–7.
7. Iannelli F, Roca MS, Lombardi R, Ciardiello C, Grumetti L, De Rienzo S, et al. Synergistic antitumor interaction of valproic acid and simvastatin sensitizes prostate cancer to docetaxel by targeting CSCs compartment via YAP inhibition. J Exp Clin Cancer Res. 2020;39(1):213.
8. Weichert W, Roske A, Gekeler V, Beckers T, Stephan C, Jung K, et al. Histone deacetylases 1, 2 and 3 are highly expressed in prostate cancer and HDAC2 expression is associated with shorter PSA relapse time after radical prostatectomy. Br J Cancer. 2008;98(3):604–10.
9. Bruzzese F, Pucci B, Milone MR, Ciardiello C, Franco R, Chianese MI, et al. Panobinostat synergizes with zoledronic acid in prostate cancer and multiple myeloma models by increasing ROS and modulating mevalonate and p38-MAPK pathways. Cell Death Dis. 2013;4(10):e878.
10. Ashburn TT, Thor KB. Drug repositioning: identifying and developing new uses for existing drugs. Nat Rev Drug Discov. 2004;3(8):673–83.
11. Salem O, Hansen CG. The Hippo pathway in prostate Cancer. Cells. 2019;8(4).

12. Liu X, Chinello C, Musante L, Cazzaniga M, Tataruch D, Calzaferri G, et al. Intraluminal proteome and peptidome of human urinary extracellular vesicles. Proteom Clin Appl. 2015;9(5–6):568–73.
13. Silva JC, Gorenstein MV, Li GZ, Vissers JP, Geromanos SJ. Absolute quantification of proteins by LCMSE: a virtue of parallel MS acquisition. Mol Cell Proteom. 2006;5(1):144–56.
14. Tyanova S, Temu T, Sinitcyn P, Carlson A, Hein MY, Geiger T, et al. The Perseus computational platform for comprehensive analysis of (prote)omics data. Nat Methods. 2016;13(9):731–40.
15. Lombardi R, Sonego M, Pucci B, Addi L, Iannelli F, Capone F, et al. HSP90 identified by a proteomic approach as druggable target to reverse platinum resistance in ovarian cancer. Mol Oncol. 2021;15(4):1005–23.
16. Huang da W, Sherman BT, Lempicki RA. Systematic and integrative analysis of large gene lists using DAVID bioinformatics resources. Nat Protoc. 2009;4(1):44–57.
17. Raudvere U, Kolberg L, Kuzmin I, Arak T, Adler P, Peterson H, et al. G:profiler: a web server for functional enrichment analysis and conversions of gene lists (2019 update). Nucleic Acids Res. 2019;47(W1):W191–8.
18. Pang Z, Chong J, Zhou G, de Lima Morais DA, Chang L, Barrette M, et al. MetaboAnalyst 5.0: narrowing the gap between raw spectra and functional insights. Nucleic Acids Res. 2021;49(W1):W388–96.
19. Liu T, Mendes DE, Berkman CE. Prolonged androgen deprivation leads to overexpression of calpain 2: implications for prostate cancer progression. Int J Oncol. 2014;44(2):467–72.
20. Li J, Xu X, Jiang Y, Hansbro NG, Hansbro PM, Xu J, et al. Elastin is a key factor of tumor development in colorectal cancer. BMC Cancer. 2020;20(1):217.
21. Gong Y, Chippada-Venkata UD, Oh WK. Roles of matrix metalloproteinases and their natural inhibitors in prostate cancer progression. Cancers (Basel). 2014;6(3):1298–327.
22. Zhang G, Miyake M, Lawton A, Goodison S, Rosser CJ. Matrix metalloproteinase-10 promotes tumor progression through regulation of angiogenic and apoptotic pathways in cervical tumors. BMC Cancer. 2014;14:310.
23. Ozden F, Saygin C, Uzunaslan D, Onal B, Durak H, Aki H. Expression of MMP-1, MMP-9 and TIMP-2 in prostate carcinoma and their influence on prognosis and survival. J Cancer Res Clin Oncol. 2013;139(8):1373–82.
24. Zhang Y, Xi S, Chen J, Zhou D, Gao H, Zhou Z, et al. Overexpression of LAMC1 predicts poor prognosis and enhances tumor cell invasion and migration in hepatocellular carcinoma. J Cancer. 2017;8(15):2992–3000.
25. Cattrini C, Barboro P, Rubagotti A, Zinoli L, Zanardi E, Capaia M, et al. Integrative Analysis of Periostin in primary and advanced prostate Cancer. Transl Oncol. 2020;13(7):100789.
26. Hu Q, Tong S, Zhao X, Ding W, Gou Y, Xu K, et al. Periostin mediates TGF-beta-Induced epithelial mesenchymal transition in prostate Cancer cells. Cell Physiol Biochem. 2015;36(2):799–809.
27. Dong Q, Fu L, Zhao Y, Du Y, Li Q, Qiu X, et al. Rab11a promotes proliferation and invasion through regulation of YAP in non-small cell lung cancer. Oncotarget. 2017;8(17):27800–11.
28. Dupont S, Morsut L, Aragona M, Enzo E, Giulitti S, Cordenonsi M, et al. Role of YAP/TAZ in mechanotransduction. Nature. 2011;474(7350):179–83.
29. Costello LC, Franklin RB. The clinical relevance of the metabolism of prostate cancer; zinc and tumor suppression: connecting the dots. Mol Cancer. 2006;5:17.
30. Fabregat A, Sidiropoulos K, Viteri G, Forner O, Marin-Garcia P, Arnau V, et al. Reactome pathway analysis: a high-performance in-memory approach. BMC Bioinformatics. 2017;18(1):142.
31. You X, Tian J, Zhang H, Guo Y, Yang J, Zhu C, et al. Loss of mitochondrial aconitase promotes colorectal cancer progression via SCD1-mediated lipid remodeling. Mol Metab. 2021;48:101203.
32. Sajnani K, Islam F, Smith RA, Gopalan V, Lam AK. Genetic alterations in Krebs cycle and its impact on cancer pathogenesis. Biochimie. 2017;135:164–72.
33. Leandro JG, Espindola-Netto JM, Vianna MC, Gomez LS, DeMaria TM, Marinho-Carvalho MM, et al. Exogenous citrate impairs glucose tolerance and promotes visceral adipose tissue inflammation in mice. Br J Nutr. 2016;115(6):967–73.
34. Silva MF, Aires CC, Luis PB, Ruiter JP, L IJ, Duran M, et al. Valproic acid metabolism and its effects on mitochondrial fatty acid oxidation: a review. J Inherit Metab Dis. 2008;31(2):205–16.
35. Lu M, Zhan X. The crucial role of multiomic approach in cancer research and clinically relevant outcomes. EPMA J. 2018;9(1):77–102.
36. Moya IM, Halder G. Hippo-YAP/TAZ signalling in organ regeneration and regenerative medicine. Nat Rev Mol Cell Biol. 2019;20(4):211–26.
37. Chen YA, Lu CY, Cheng TY, Pan SH, Chen HF, Chang NS. WW Domain-Containing proteins YAP and TAZ in the Hippo Pathway as key regulators in Stemness Maintenance, tissue homeostasis, and Tumorigenesis. Front Oncol. 2019;9:60.
38. Santos DM, Pantano L, Pronzati G, Grasberger P, Probst CK, Black KE, et al. Screening for YAP inhibitors identifies statins as modulators of fibrosis. Am J Respir Cell Mol Biol. 2020;62(4):479–92.
39. Hao F, Xu Q, Wang J, Yu S, Chang HH, Sinnett-Smith J, et al. Lipophilic statins inhibit YAP nuclear localization, co-activator activity and colony formation in pancreatic cancer cells and prevent the initial stages of pancreatic ductal adenocarcinoma in KrasG12D mice. PLoS ONE. 2019;14(5):e0216603.
40. Koohestanimobarhan S, Salami S, Imeni V, Mohammadi Z, Bayat O. Lipophilic statins antagonistically alter the major epithelial-to-mesenchymal transition signaling pathways in breast cancer stem-like cells via inhibition of the mevalonate pathway. J Cell Biochem. 2019;120(2):2515–31.
41. Mi W, Lin Q, Childress C, Sudol M, Robishaw J, Berlot CH, et al. Geranylgeranylation signals to the Hippo pathway for breast cancer cell proliferation and migration. Oncogene. 2015;34(24):3095–106.
42. Huang J, Zhang L, Wan D, Zhou L, Zheng S, Lin S, et al. Extracellular matrix and its therapeutic potential for cancer treatment. Signal Transduct Target Ther. 2021;6(1):153.
43. Jang HS, Lal S, Greenwood JA. Calpain 2 is required for glioblastoma cell invasion: regulation of matrix metalloproteinase 2. Neurochem Res. 2010;35(11):1796–804.
44. Bhat KM, Setaluri V. Microtubule-associated proteins as targets in cancer chemotherapy. Clin Cancer Res. 2007;13(10):2849–54.
45. Lin C, Blessing AM, Pulliam TL, Shi Y, Wilkenfeld SR, Han JJ, et al. Inhibition of CAMKK2 impairs autophagy and castration-resistant prostate cancer via suppression of AMPK-ULK1 signaling. Oncogene. 2021;40(9):1690–705.
46. Sorrentino G, Ruggeri N, Zannini A, Ingallina E, Bertolio R, Marotta C, et al. Glucocorticoid receptor signalling activates YAP in breast cancer. Nat Commun. 2017;8:14073.
47. Li Y, Wang J, Zhong W. Regulation and mechanism of YAP/TAZ in the mechanical microenvironment of stem cells (review). Mol Med Rep. 2021;24(1).
48. Zanconato F, Cordenonsi M, Piccolo S. YAP and TAZ: a signalling hub of the tumour microenvironment. Nat Rev Cancer. 2019;19(8):454–64.
49. Shi X, Young CD, Zhou H, Wang X. Transforming growth factor-beta signaling in Fibrotic diseases and Cancer-Associated fibroblasts. Biomolecules. 2020;10(12).
50. Noguchi S, Saito A, Nagase T. YAP/TAZ signaling as a Molecular Link between Fibrosis and Cancer. Int J Mol Sci. 2018;19(11).
51. Wu F, Yang J, Liu J, Wang Y, Mu J, Zeng Q, et al. Signaling pathways in cancer-associated fibroblasts and targeted therapy for cancer. Signal Transduct Target Ther. 2021;6(1):218.
52. Liu P, Zhang C, Liao Y, Liu J, Huang J, Xia M, et al. High expression of PTPRM predicts poor prognosis and promotes tumor growth and lymph node metastasis in cervical cancer. Cell Death Dis. 2020;11(8):687.
53. Vallianou NG, Kostantinou A, Kougias M, Kazazis C. Statins and cancer. Anticancer Agents Med Chem. 2014;14(5):706–12.
54. Frick M, Dulak J, Cisowski J, Jozkowicz A, Zwick R, Alber H, et al. Statins differentially regulate vascular endothelial growth factor synthesis in endothelial and vascular smooth muscle cells. Atherosclerosis. 2003;170(2):229–36.
55. Tate R, Zona E, De Cicco R, Trotta V, Urciuoli M, Morelli A, et al. Simvastatin inhibits the expression of stemness–related genes and the metastatic invasion of human cancer cells via destruction of the cytoskeleton. Int J Oncol. 2017;51(6):1851–9.
56. Cai Z, Deng Y, Ye J, Zhuo Y, Liu Z, Liang Y, et al. Aberrant expression of citrate synthase is linked to Disease Progression and clinical outcome in prostate Cancer. Cancer Manag Res. 2020;12:6149–63.
57. Abdel-Mawgoud AM, Lepine F, Deziel E. A chiral high-performance liquid chromatography-tandem mass spectrometry method for the stereospecific analysis of enoyl-coenzyme A hydratases/isomerases. J Chromatogr A. 2013;1306:37–43.
58. Zhang J, Ibrahim MM, Sun M, Tang J. Enoyl-coenzyme A hydratase in cancer. Clin Chim Acta. 2015;448:13–7.
59. Paiva H, Thelen KM, Van Coster R, Smet J, De Paepe B, Mattila KM, et al. High-dose statins and skeletal muscle metabolism in humans: a randomized, controlled trial. Clin Pharmacol Ther. 2005;78(1):60–8.
60. Salimi A, Gholamifar E, Naserzadeh P, Hosseini MJ, Pourahmad J. Toxicity of lithium on isolated heart mitochondria and cardiomyocyte: a justification for its cardiotoxic adverse effect. J Biochem Mol Toxicol. 2017;31(2).
61. Sciacovelli M, Frezza C, Oncometabolites. Unconventional triggers of oncogenic signalling cascades. Free Radic Biol Med. 2016;100:175–81.

62. Dalla Pozza E, Dando I, Pacchiana R, Liboi E, Scupoli MT, Donadelli M, et al. Regulation of succinate dehydrogenase and role of succinate in cancer. Semin Cell Dev Biol. 2020;98:4–14.
63. Sircar K, Huang H, Hu L, Cogdell D, Dhillon J, Tzelepi V, et al. Integrative molecular profiling reveals asparagine synthetase is a target in castration-resistant prostate cancer. Am J Pathol. 2012;180(3):895–903.
64. Zhang LF, Liu LS, Chu XM, Xie H, Cao LJ, Guo C, et al. Combined effects of a high-fat diet and chronic valproic acid treatment on hepatic steatosis and hepatotoxicity in rats. Acta Pharmacol Sin. 2014;35(3):363–72.
65. Malenda A, Skrobanska A, Issat T, Winiarska M, Bil J, Oleszczak B, et al. Statins impair glucose uptake in tumor cells. Neoplasia. 2012;14(4):311–23.
66. Khan S, Jena G. Valproic acid improves glucose homeostasis by increasing Beta-cell proliferation, function, and reducing its apoptosis through HDAC inhibition in Juvenile Diabetic Rat. J Biochem Mol Toxicol. 2016;30(9):438–46.
67. Rakitin A. Does Valproic Acid have potential in the treatment of diabetes Mellitus? Front Endocrinol (Lausanne). 2017;8:147.
68. Kumar D, Gupta A, Mandhani A, Sankhwar SN. Metabolomics-derived prostate cancer biomarkers: fact or fiction? J Proteome Res. 2015;14(3):1455–64.
69. Jiang Y, Cheng X, Wang C, Ma Y. Quantitative determination of sarcosine and related compounds in urinary samples by liquid chromatography with tandem mass spectrometry. Anal Chem. 2010;82(21):9022–7.
70. Koutros S, Meyer TE, Fox SD, Issaq HJ, Veenstra TD, Huang WY, et al. Prospective evaluation of serum sarcosine and risk of prostate cancer in the prostate, lung, colorectal and ovarian Cancer Screening Trial. Carcinogenesis. 2013;34(10):2281–5.
71. Koo JH, Guan KL. Interplay between YAP/TAZ and metabolism. Cell Metab. 2018;28(2):196–206.
72. Elisi GM, Santucci M, D'Arca D, Lauriola A, Marverti G, Losi L et al. Repurposing of drugs targeting YAP-TEAD functions. Cancers (Basel). 2018;10(9).

Publisher's note